Available online at www.sciencedirect.com
SCIENCE DIRECT®
Journal of Power Sources 145 (2005) 206–215
JOURNAL OF POWER SOURCES
www.elsevier.com/locate/jpowsour

Electrochemical and microstructural characterization of the redox tolerance of solid oxide fuel cell anodes

D. Waldbillig [a,*], A. Wood [b], D.G. Ivey [a]

[a] *Department of Chemical and Materials Engineering, University of Alberta, Edmonton, AB, Canada T6G 2G6*
[b] *Versa Power Systems, Ltd., 4852 52 St SE, Calgary, AB, Canada T2B 3R2*

Accepted 21 December 2004
Available online 23 May 2005

Abstract

The most commonly used solid oxide fuel cell (SOFC) anode material is a two phase nickel and yttria stabilized zirconia (Ni/YSZ) cermet. During typical fuel cell operation, this material remains a cermet; however, the anode may reoxidize in a commercial SOFC system due to seal leakage, fuel supply interruption, or system shutdown. The cyclic reduction and oxidation (redox) of nickel will result in large bulk volume changes, which may have a significant effect on the integrity of interfaces within the fuel cell and thus may cause significant performance degradation.

A baseline of the redox behaviour of an anode-supported SOFC was developed using electrochemical testing and electron microscopy. During redox tests, the cell's initial performance was characterized and then a small amount of air was blown over the anode in order to reoxidize the cell. The cell was then reduced and the electrochemical performance was remeasured in order to determine the amount of redox degradation. Cell performance decreased slightly after each redox cycle, especially for redox times greater than 1 hour. The microstructural changes that occurred after redox cycling were characterized using scanning and transmission electron microscopy (SEM and TEM). Redox cycling significantly changed the microstructure of the anode substrate in the cell.

Keywords: Solid oxide fuel cells; Redox; Anode; Oxidation; Electron microscopy

1. Introduction

Fuel cells are a clean, efficient energy generation technology that produces electricity by the direct electrochemical combination of a fuel with an oxidant. This direct production of electricity effectively bypasses the conversion of the fuel's chemical energy into thermal and mechanical energy and thus allows higher theoretical efficiencies to be achieved.

Solid oxide fuel cells (SOFC) are a type of fuel cell that uses a solid, ionically conducting ceramic oxide as an electrolyte. Due to the inherently low ionic conductivity of the solid electrolytes at lower temperatures, these cells are typically operated at temperatures between 600 and 1000 °C.

The most commonly used SOFC anode material is a two phase, nickel and yttria stabilized zirconia (Ni/YSZ) cermet. During fuel cell operation, this material is exposed to a reducing environment and thus remains a cermet. However, the metallic component of the anode may reoxidize in a commercial SOFC system due to seal leakage, fuel supply interruption or system shutdown. A reoxidized cell must be reduced prior to operation. Thus, cyclic reduction and oxidation (redox) of the anode is likely to occur during commercial SOFC operations. The reduction and oxidation of nickel will result in large bulk volume changes, which may have a significant effect on the integrity of interfaces within a fuel cell and thus result in performance degradation.

System redox solutions, such as the use of a reducing purge gas, are possible, but are cumbersome and expensive. Another possible redox solution is to change the anode material to a substance that is not as susceptible to oxidation, such as a

* Corresponding author. Tel.: +1 403 204 6113; fax: +1 403 204 6102.
E-mail address: djw3@ualberta.ca (D. Waldbillig).

0378-7753/$ – see front matter © 2005 Elsevier B.V. All rights reserved.
doi:10.1016/j.jpowsour.2004.12.071

ceramic oxide; however, there are currently few alternative anode materials that exhibit equivalent performance to the state-of-the-art Ni/YSZ materials system. Thus, if the anode material remains unchanged and system redox solutions are deemed too expensive, the only remaining way to enhance SOFC redox tolerance is to modify the microstructure of the anode.

A few groups [1–4] have published kinetic studies of the Ni/YSZ system or have looked at the change in anode dimensions after redox cycling. Fouquet et al. [2] have been the only group thus far to report electrochemical results and noted that the polarization resistance of cells increased after redox cycling. However, no group has to date performed a systematic study of the effect of redox cycling on the microstructure and performance of anode-supported SOFC. This study characterizes the electrochemical performance degradation and microstructural changes that occur after redox cycling an anode-supported SOFC produced using Versa Power Systems Ltd.'s (VPS, formerly Global Thermoelectric) TSC-2 cell production process.

2. Experimental methods

2.1. Fuel cell preparation

Versa Power Systems Ltd.'s (VPS's) standard TSC-2 cell manufacturing process was used to fabricate fuel cell samples. This process is made up of three major unit operations: tape casting, screen printing and co-firing [5].

The anode substrate was produced via a single layer tape cast process. Powders were dispersed to form a slurry, followed by milling to get the proper particle size and morphology and to thoroughly mix the components. After grinding and mixing, the slurries were tape cast on VPS's 20 m tape caster. The cast tape was dried and then cut into individual pieces. Anode substrate samples were fired directly after tape cutting. No additional layers were deposited on these samples.

After the tape was cut, the anode functional layer, electrolyte and cathode layers were screen printed onto each green (unfired) anode substrate piece. After the layers were printed, the tape was punched to the appropriate cell size.

The final processing step involved one-step co-firing of all cell components. This action combines binder burnout, high temperature co-sintering and cooling into a single firing step.

2.2. Redox treatment techniques

2.2.1. Anode substrate samples

Anode substrate samples were redox cycled externally in a furnace. The samples were reduced in 5% hydrogen (95% argon or nitrogen) and oxidized in air at a temperature of 700 °C for varying amounts of time to simulate redox cycling conditions. Two treatment conditions were desired: full reduction/oxidation and partial reduction/oxidation. Samples to be characterized by SEM were redox cycled as bulk samples and then were fractured in order to examine the anode microstructure. Samples to be characterized by TEM were prepared as planar TEM specimens, using the procedure detailed in Section 2.4.2, and then were redox cycled.

2.2.2. Fuel cell samples

Fuel cell samples were redox cycled in a single-cell test stand at 750 °C. After measuring the baseline current–voltage response and operating the cell under steady-state current load, the cell was unloaded and then oxidized by blowing a low flow rate of air (0.12 SLPM) across the anode in order to slowly oxidize the nickel. The low air flow rate simulates a worst case scenario of the condition in which the fuel supply is interrupted and air leaks into the anode cavity. After redox cycling, the cell was reduced over a period of 4 h in hydrogen at 750 °C. After reduction was complete, current–voltage curves were measured and the cell was loaded to a constant current density and then held under this condition for a minimum of 15 h in order to determine the amount of degradation caused by redox cycling. Redox cycles of 20 min (10% redox depth), 40 min (20% redox depth), 60 min (30%), 120 min (60%), 240 min (120%, i.e., excess air flow) and 360 min (180%, i.e., excess air flow) in length were performed during the redox tests.

2.2.3. Redox depth approach

A theoretical redox depth strategy has been developed in order to better define exactly how much oxidation should occur. This analysis uses the amount of Ni within the cell and the flow rate of air to predict the amount of time it should take to oxidize the cell to a specific redox depth assuming that all oxygen that passes through the anode during the redox cycle reacts to form NiO. The approach assumes an ideal situation where all oxygen entering the anode chamber during the test is consumed by nickel in the cell. In practice, this will depend on a number of factors including the gas flow rates, temperature, flow field configuration and other test specific factors. Therefore, the validity of this assumption was verified using gas chromatography (GC) analysis to measure the amount of oxygen in the outlet gas during redox cycles. According to this approach a redox time of approximately 200 min corresponded to a redox depth of 100% or a fully oxidized cell.

2.3. Electrochemical testing methods

2.3.1. Test station description

VPS has a number of custom designed single-cell test stations. Each test stand is fully automated and controlled using Labview and is able to reliably test a fuel cell under a number of conditions. The experiments used a testing configuration with stainless steel test jigs and cross flow fuel (H_2) and oxidant (air) delivery. Standard TSC-2 10 cm × 10 cm (81 cm^2 active area) production cells with stainless steel test jigs and the same seals and current collection as used in VPS's SOFC stacks were used for all tests. This testing setup pro-

vided a commercially realistic testing configuration, as no precious metal contact materials or current collectors were used, and no special furnace or sealing configurations were required.

Power densities as high as 1.4 W/cm^2 have been achieved previously at 0.7 V and 750 °C using this testing configuration [5].

2.3.2. Current–voltage (I–V) curve tests

During an *I–V* curve test, high fuel and air flows were used and the current was stepped slowly from 0 to 60 A (0.74 A/cm^2). Tests were performed at 750 °C using H_2 fuel with a humidity of approximately 3%. These tests have three main purposes:

1. To characterize the open circuit voltage (OCV) of the cell in order to ensure that there is little cross-leak or electronic conductivity in the electrolyte and that there is a good seal between components.
2. To measure the electrochemical performance of the cell at a high current density (0.74 A/cm^2 or 60 A) before and after redox cycling.
3. To examine the shape of the *I–V* curve before and after redox cycling in order to roughly determine the amount of activation, ohmic and mass transport losses and whether the proportion of each type of loss changes after redox cycling.

2.3.3. Steady-state hold tests

Steady-state hold tests were performed to measure the electrochemical performance of the cell at a fixed current and fuel/air utilization after redox cycling and to ensure that the measured performance is stable. The tests were performed at 750 °C and 40.5 A (0.5 A/cm^2) in humidified hydrogen. A fuel utilization of 54% and air utilization of 27% was used for the tests. These conditions were held for a minimum of 15 h.

2.4. Electron microscopy

2.4.1. Scanning electron microscopy (SEM)

Scanning electron microscopy was used to characterize the microstructural changes that occurred after redox cycling. All SEM images were taken using a LEO 1450 variable pressure SEM operating at 15 kV with an Oxford Instruments ultra thin window (UTW) energy-dispersive x-ray (EDX) spectrometer.

All samples examined in the SEM were cross-sections that were prepared as fresh fractures by breaking the cell into pieces. Some samples were examined as fresh fractures after a thin gold coating was applied to minimize charging effects. Other fracture samples were mounted in epoxy and polished with SiC paper, diamond paste and an Al_2O_3 suspension in order to provide a flat, easy to image surface.

2.4.2. Transmission/scanning transmission electron microscopy

TEM images were obtained using either a JEOL-2010 TEM with a Noran UTW EDX spectrometer or a Tecnai F20 field emission gun (FEG) TEM/STEM with an EDAX Phoenix UTW EDX spectrometer.

Both planar and cross-sectional TEM samples were prepared. Cross-sectional samples were prepared by gluing together sectioned pieces using epoxy. After gluing, both sample types were prepared in a similar fashion. The basic TEM sample preparation method used mechanical polishing, dimpling and sputtering techniques. A 3 mm diameter disk was cut from a sample using an ultrasonic cutter. The disk was then ground and polished to a thickness of less than 200 μm using 320 and 600 grit silicon carbide paper. After polishing, the disk was dimpled to a central thickness of less than 20 μm using a bronze wheel and diamond paste. In a dimpler, a rotating wheel was used to grind a dimple-like depression on each side of the sample. This resulted in a sample with a thick outer edge for mechanical support and a thin central area. After dimpling, an ion mill was used to sputter away the mechanical damage induced by polishing/dimpling and to further thin the sample to perforation. Argon ions accelerated at 5–6 keV, impinging at 15° to the sample surface, were utilized for sputtering. After this treatment the thin area around the hole is ∼100–200 nm in thickness and thus will be electron transparent.

3. Results

3.1. Baseline electrochemical tests

After redox cycling, current–voltage (*I–V*) curves and steady-state hold tests were used to characterize the amount of electrochemical performance degradation that occurred. All tests were performed at 750 °C.

3.1.1. I–V curve tests

The shape of an *I–V* curve will give an approximate break down of the activation, ohmic and mass transport losses that occur during the test. As well, *I–V* curve tests are used to measure the cell's performance under higher current but low utilization conditions. The *I–V* curve for one of the baseline redox tests (Sample 1) is shown in Fig. 1. It can be seen in the figure that the performance decreases slightly after each redox cycle, but significant amounts of degradation do not occur until after the 1 h redox cycle. The largest drop in performance occurs after the 4 h redox cycle, likely because this is the first redox cycle that fully oxidizes the cell. The average cumulative amount of voltage degradation after the standard redox test is 0.089 ± 0.001 V or $10.9 \pm 0.1\%$.

3.1.2. Steady-state hold tests

Steady-state hold tests were performed at lower currents and intermediate utilization conditions to ensure that the mea-

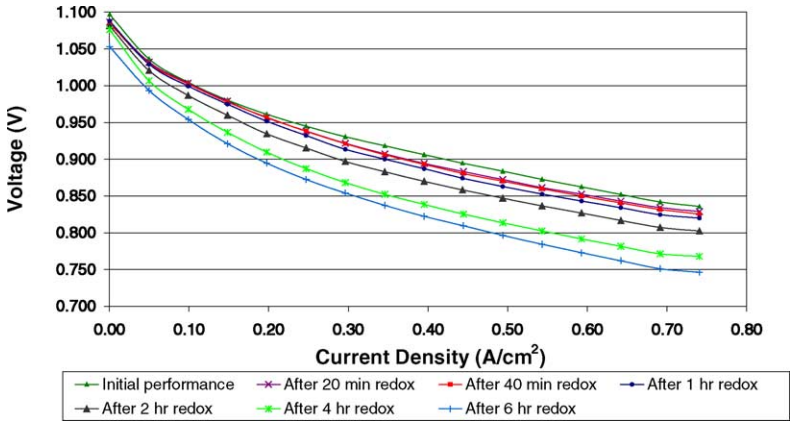

Fig. 1. *I–V* curves comparing the performance before and after redox cycling.

sured performance was stable and to provide another measure of the amount of performance degradation after redox cycling. The steady-state hold test for one baseline redox test (Sample 1) is shown in Fig. 2. In the figure, the arrows indicate the point at which each redox cycle occurs (break in the voltage versus time line), while the line indicates the initial cell voltage and shows the measured cell voltage after each redox cycle under the test conditions specified in Section 2.3.3. The current load is removed during oxidation and reduction. The degradation behaviour of the sample followed a similar trend to that seen during *I–V* curve tests. Cell performance decreased slightly after each redox cycle, but significant amounts of degradation did not really occur until after the 1 h redox cycle. The largest performance drop again occurred after the 4 h redox cycle. After longer redox cycles (4 and 6 h) the performance seemed to increase slightly before stabilizing. This effect may be an indication that the 4 h reduction period is not quite long enough to fully reduce the cell for the testing conditions utilized, even though the thermogravimetric results suggested otherwise. The average cumulative amount of voltage degradation after the standard redox test is 0.072 ± 0.004 V or $8.9 \pm 0.6\%$.

3.2. Verification of redox depth approach

The validity of the redox depth approach was verified using two methods: by observing the behaviour of the cell voltage during oxidation, i.e., the length of time required for the voltage to decrease to a value of 0 V, and by measuring the amount of oxygen in the fuel outlet stream during oxidation, using gas chromatography.

3.2.1. Voltage behaviour during oxidation

Fig. 3 shows the behaviour of the voltage during oxidation at OCV. The voltage initially rapidly decreases until it reaches a value of approximately 0.7 V. The voltage then decreases at a fairly constant rate until it reaches a value of 0 V after about 3.5 h. A voltage value of 0 should indicate that the cell is mostly oxidized, i.e., there should be no electrical connection between Ni/NiO particles. This supports the redox depth calculations that indicate that 100% redox depth should occur after approximately 200 min.

It can be seen in Fig. 3 that 4 and 6 h redox cycles will result in complete oxidation of the cell during baseline redox tests.

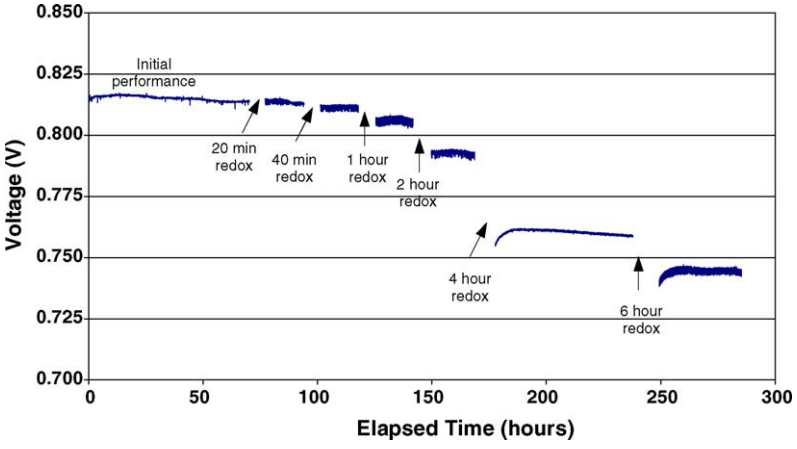

Fig. 2. Steady-state hold tests comparing the performance before and after redox cycling.

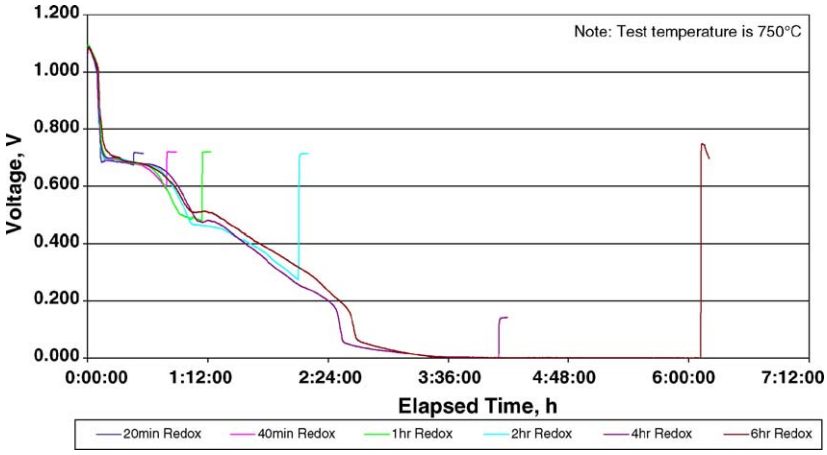

Fig. 3. Voltage behaviour during cell oxidation.

3.2.2. Gas chromatography (GC)

Gas chromatography (GC) was performed in order to measure the amount of oxygen present in the anode outlet stream during oxidation. The test results showed that during oxidation at 750 °C there was no oxygen present in the anode exhaust until after approximately 2 h of oxidation. After 2 h an oxygen concentration of about 1% O_2 was present in the outlet stream. The amount of oxygen gradually increased until the oxygen content was about 20% after 6 h. This indicates that the calculated time to redox depths greater than 60% (2 h oxidation) will be slightly lower than the actual time, since some of the oxygen is exhausted in the outlet gas stream rather than being used up to oxidize the Ni in the cell. The time calculated for redox depths lower than 60% (120 min) should be accurate.

3.3. Electron microscopy

3.3.1. Anode substrate samples

Externally reduced anode substrate samples were examined to look at the effect of redox cycling on the relatively coarse microstructure of the anode substrate. The anode substrate is very thick when compared to the other fuel cell layers, so the redox behaviour of this layer may have a significant effect on the rest of the cell.

3.3.1.1. As prepared microstructure. Fig. 4 shows a backscattered electron (BSE) SEM image of a fresh fractured, as prepared (oxidized) microstructure. The YSZ phase is light in colour, with a grain size around 1 μm, while the NiO grains appear grey and are several microns in size.

Fig. 5 is a bright field (BF) TEM image of an as prepared sample and provides confirmation of the SEM results. The pores and holes in the BF image appear white. Selected area electron diffraction (SAD) (insets in Fig. 5) and energy-dispersive x-ray analysis (EDX) techniques were used to confirm the phases present, i.e., NiO and YSZ.

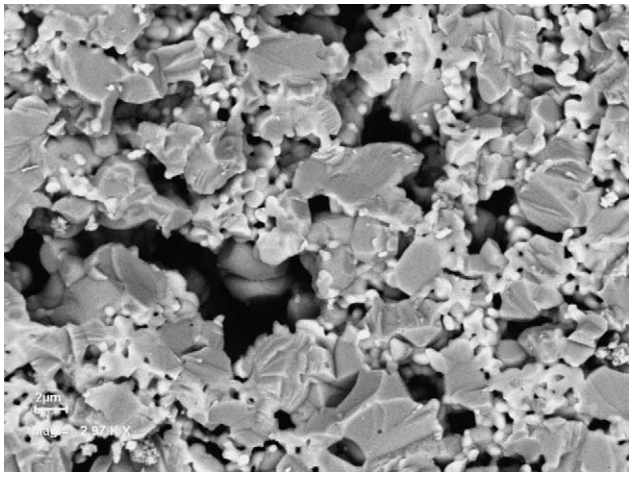

Fig. 4. BSE SEM image of a fresh fractured, as prepared (oxidized) sample.

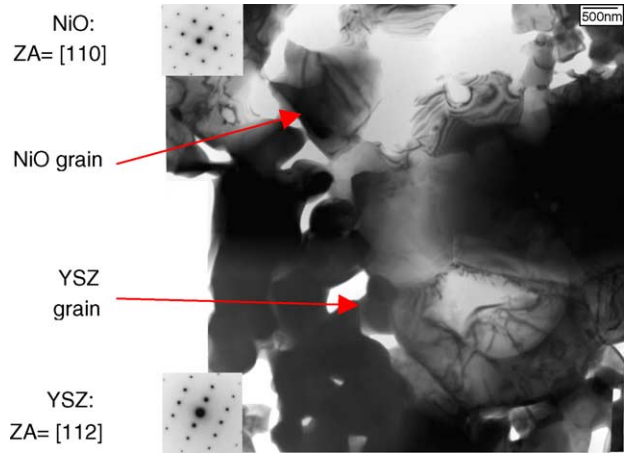

Fig. 5. BF TEM image of an as prepared sample.

3.3.1.2. Reduced microstructure. Fig. 6 is a BSE SEM image of a fully reduced, fresh fractured anode and shows the individual Ni grains, which are several microns in size, in a larger Ni particle and the small YSZ grains, which are com-

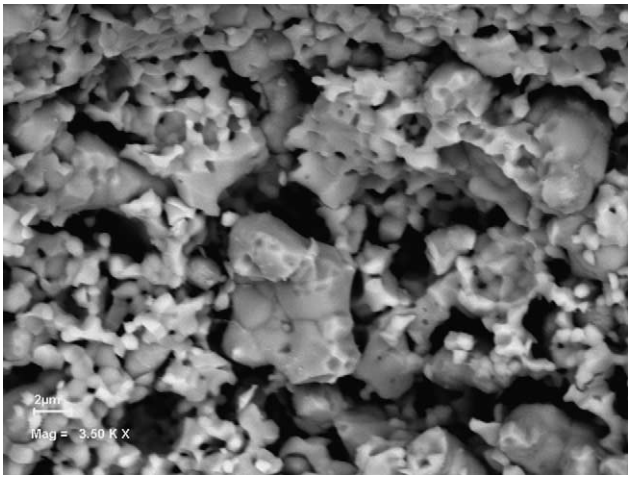

Fig. 6. BSE SEM image of a fresh fractured, fully reduced sample.

pletely unaffected by the entire reduction process. It is apparent from the image that the amount of porosity has increased after reduction.

Fig. 7 is a BF TEM micrograph of a partially reduced NiO/YSZ anode. This image clearly shows the distribution of reduced Ni and unaffected YSZ within the sample. The sample had been heated to 700 °C in 5% H_2 for 5 min. The image shows the presence of small (50 nm) intragranular pores within the larger Ni grain. The grain, which is several microns in size, is single crystalline, as illustrated by the SAD pattern in the inset. The intragranular porosity likely helps to accommodate the large volume change (~40%) associated with NiO reduction to Ni without overstressing the YSZ particles, which are unaffected by the reduction process.

The diffraction pattern of the partially reduced sample (inset of Fig. 7) contains satellite spots, which indicate that multiple diffraction is occurring. The more intense spots in the diffraction pattern correspond to nickel while the satellite spots correspond to both Ni and NiO reflections. The presence of satellite spots indicates that the grain is only partially reduced and that Ni is growing epitaxially on the parent NiO

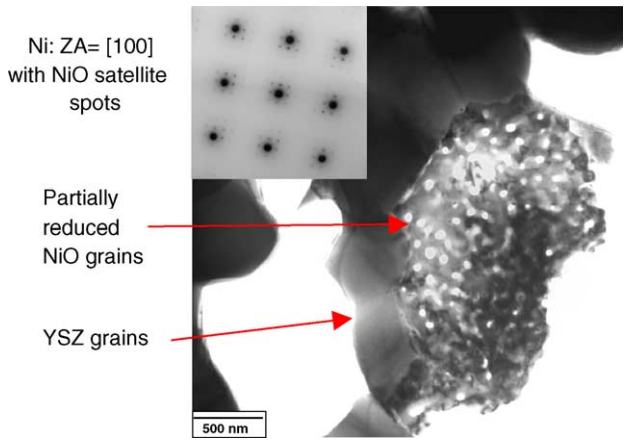

Fig. 7. BF TEM image of a partly reduced sample.

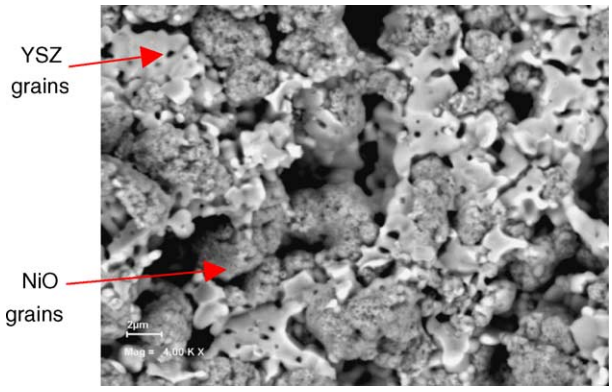

Fig. 8. BSE SEM image of a reoxidized sample.

grain. Diffraction patterns of several orientations from various grains were obtained and all patterns contained satellite spots. When the sample is fully reduced the satellite spots disappear, leaving only a single Ni pattern.

Epitaxial growth of Ni on the NiO grains is somewhat unexpected due to the large mismatch (15.6%) in lattice parameters between Ni and NiO [6], but not unheard of, as Kuhlenbeck and Freund have reported epitaxial growth of NiO on Ni substrates for ultrathin films [7].

3.3.1.3. Reoxidized microstructure. Fig. 8 is a BSE SEM image of fully reoxidized, fresh fractured anode sample. After reoxidation, the NiO grains appear spongy with much smaller pores than the as prepared, oxidized samples before redox cycling.

TEM imaging (Fig. 9) of reoxidized samples show an interesting result – the formation of very fine grains of NiO less than 100 nm in size. The YSZ grains appear to be unaffected by the reduction and reoxidation process. These samples were fully reduced for a period of 5 h at 700 °C and then reoxidized for 15 min at 700 °C.

The presence of the fine NiO grains was confirmed by the appearance of the polycrystalline ring diffraction pattern seen in the inset of Fig. 9. The pattern shows little orientation

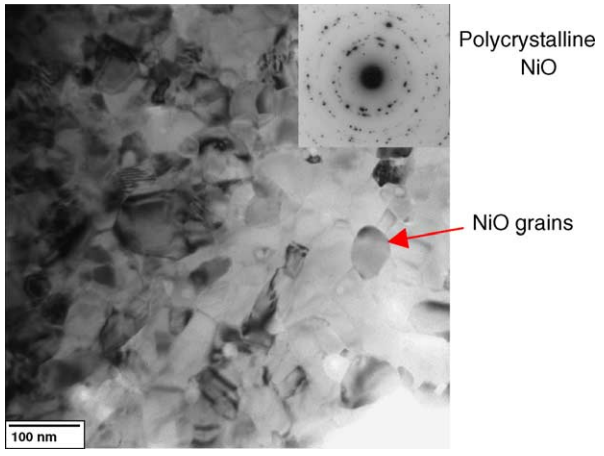

Fig. 9. BF TEM image of a reoxidized sample.

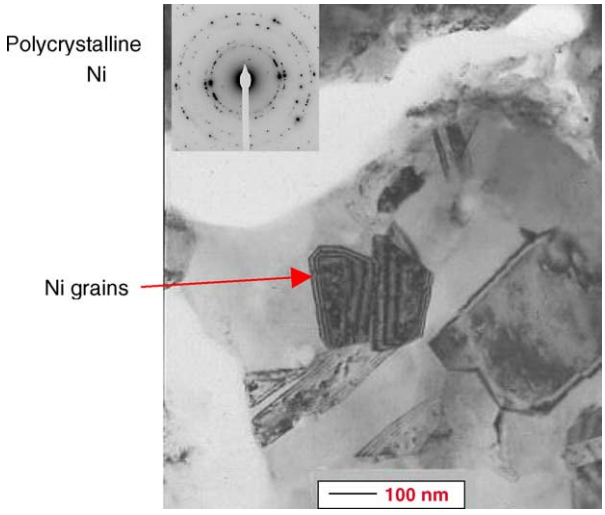

Fig. 10. BF TEM image of a rereduced sample.

effects, indicating that preferred growth of NiO grains on the Ni does not occur. These grains were completely reoxidized as no additional Ni rings were observed in the diffraction pattern.

3.3.1.4. Rereduced microstructure. After rereduction, the overall Ni grain size remains small (<200 nm) as can be seen in Fig. 10. The presence of fine Ni grains was confirmed by the polycrystalline ring diffraction pattern seen in the inset of Fig. 10. No preferred orientation was evident. The sample area characterized was completely reduced, as no additional NiO rings were present in the diffraction pattern. These samples were fully reduced for a period of 5 h, fully reoxidized for a period of 8 h and then rereduced for 1 h. Redox cycles were performed at a temperature of 700 °C.

3.3.2. Fuel cell samples

The microstructure of fuel cell samples prepared using VPS's TSC-2 cell production process was examined after redox cycling in a single-cell test stand. Analysis of the microstructure of these samples served to look at the effect of redox cycling on the integrity of the electrolyte and cell interfaces, the microstructure of the anode functional layer (AFL) and to confirm the observations of the anode substrate samples.

An oxidized fuel cell sample after redox cycling is shown in Fig. 11. The microstructure of the AFL does not appear to have been significantly affected by redox cycling. The only difference between the AFL in a reduced and oxidized state appears to be that the AFL is slightly more porous in the reduced state which is to be expected due the volume changes induced when NiO reduces. Fig. 12 shows a higher magnification image of the anode substrate of the sample. The spongy NiO structure typical of reoxidized anode substrate samples can easily be seen in the figure.

Redox cycling will likely cause two distinct types of degradation in fuel cell samples: mechanical damage due to the expansion of Ni as it oxidizes and microstructural damage. The first type of damage is easy to characterize, as it will likely result in electrolyte cracks or in delamination of fuel cell layers. The second type is much more difficult to investigate, since there is no general agreement on what constitutes a good anode microstructure. Therefore, it will be difficult to conclusively determine whether the microstructural changes caused by redox actually result in performance degradation.

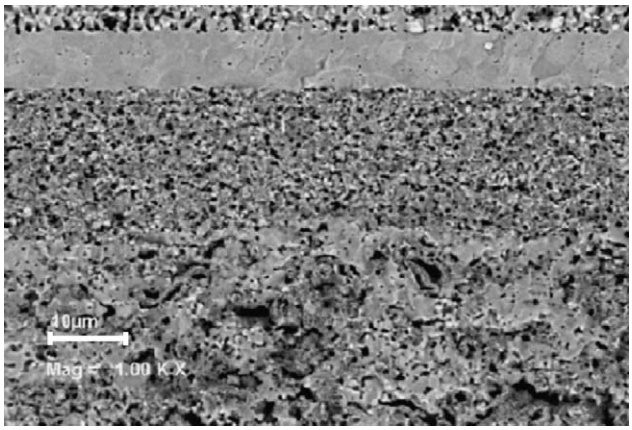

Fig. 11. SEM BSE image of a fresh fractured, reoxidized anode-supported SOFC.

Fig. 13 shows an electrolyte crack caused by redox cycling. The crack is likely caused by the volume expansion exhibited by the AFL during oxidation.

Fig. 14 shows microstructural damage likely caused by redox cycling. The sample shown in the figure was redox cycled, rereduced and cooled in nitrogen to preserve the microstructure. The redox process appears to have damaged the AFL microstructure as the anode substrate near the damage has remained oxidized while the rest of the anode substrate is in a reduced state. This was the only type of microstructural damage seen in fuel cell samples.

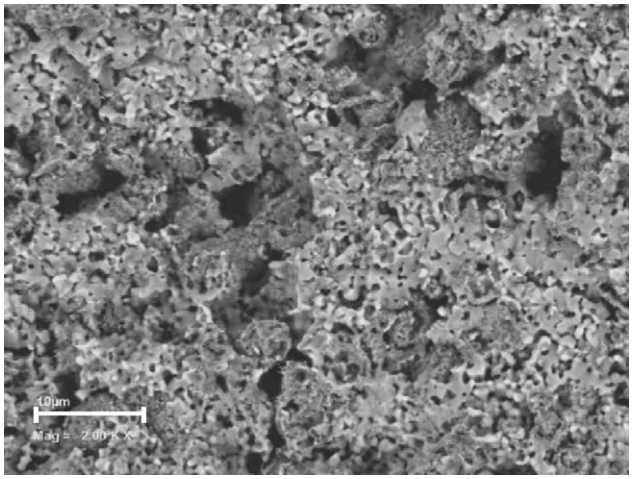

Fig. 12. Higher magnification SEM BSE image of the cell in Fig. 11.

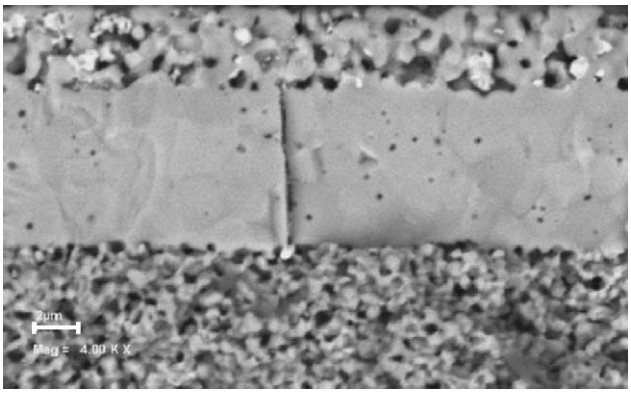

Fig. 13. SEM BSE image of a large vertical electrolyte crack in a fresh fractured anode-supported SOFC after redox cycling.

4. Discussion

4.1. Electrochemical results

The electrochemical test results were reproducible and both *I–V* curves and steady-state hold tests had very similar results. Table 1 shows the average amount of degradation seen after each redox cycle for baseline redox tests. It can be seen that the amount of degradation increases as the redox time i.e. redox depth increases. Little degradation occurs at short redox times (<60 min), but from visual observations of cells that were partially oxidized and cooled in inert gas to preserve the oxidized microstructure, it is clear that the oxidation of the cell is uneven with more oxidation of the anode substrate occurring than AFL due to the gas flow arrangement of the test jig. This indicates that redox cycling does not significantly increase the contact resistance between the anode and the anode interconnect for this testing configuration and that oxidation of the anode substrate is unlikely to be the major cause of degradation. The maximum amount of degradation was seen after the 240 min redox cycle. This is likely due to the fact that this is the first redox cycle to completely reoxidize the anode and AFL (>100% redox depth). After the first 100% redox depth cycle the amount of redox degradation after full oxidation lessens. This may indicate that further 100% redox cycles will not degrade the performance as significantly as the first one does, and that it is likely that AFL oxidation is the major cause of electrochemical performance degradation. The cumulative amount of performance degradation seen after six redox cycles (840 min total redox time) was slightly lower for steady-state hold tests compared with *I–V* curve tests. This trend may be a result of the lower current density used for steady-state hold tests.

The overall shape of the *I–V* curve (Fig. 1) does not significantly change after redox cycling, which suggests that redox cycling does not predominantly introduce one type of loss mechanism. It can also be seen in the figure that the current during this test does not reach the limit of mass transport losses; therefore, only activation and ohmic losses are present in this test.

The rate and depth of oxidation and the amount of redox degradation are likely dependent on the testing configuration and on conditions such as the gas flow rates, temperature, or flow field configuration.

4.2. Microstructural results

SEM results were very consistent for externally redox cycled anode substrate samples and fuel cell samples redox

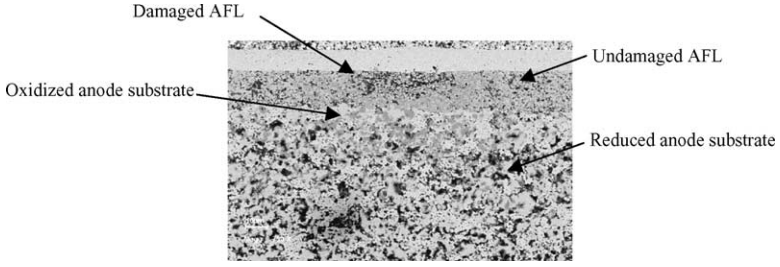

Fig. 14. SEM BSE image of a polished anode-supported SOFC after redox cycling with AFL microstructural damage.

Table 1
The average amount of degradation after each redox cycle

Redox time (min)	Redox depth (%)	Degradation after redox cycling for *I–V* curve tests (%)	Degradation after redox cycling for steady-state hold tests (%)
20	10	−0.7	−0.1
40	20	−0.7	−0.3
60	30	−1.0	−0.7
120	60	−1.6	−1.6
240	120	−4.2	−4.5
360	180	−2.8	−1.7
840	–	−10.9	−8.9

cycled in single-cell test stands. For both sample types the porosity was significantly increased after reduction and the same spongy microstructure was seen after reoxidation. This spongy microstructure is very different than the as prepared (oxidized) microstructure and is likely caused by the expansion of the nickel component of the anode during oxidation. After the first redox cycle, this spongy structure is always seen when the cell is in the reoxidized state, which indicates that the redox induced microstructural change is more or less permanent.

Thermomechanical analysis (TMA) performed in a previous study [4] showed that neither the anode substrate, nor the electrolyte, changed dimensions during oxidation while the AFL expanded during oxidation. Thus, as the AFL expands during oxidation, it is constrained by the electrolyte and anode substrate layers and stress builds up. If these stresses become too severe, the dense electrolyte may fracture as seen in Fig. 13. The open circuit voltage of some cells did decrease somewhat after longer redox cycles (4 and 6 h), which indicates that redox cycling likely produces some electrolyte cracking. Delamination of fuel cell layers was not seen in any of the redox cycled cells.

The grain refinement that occurs upon reoxidation of TEM samples may be due to the large number of intragranular pores that occur after reduction. These pores provide many nucleation sites for the NiO grains to form and thus promote the formation of small randomly oriented grains. Epitaxial growth of Ni on NiO grains, intragranular porosity within the Ni grains upon reduction and the recrystallization of very small (<100 nm) grains after reoxidation was not seen in bulk redox cycled samples. These phenomena may be caused by the extreme thinness of the redox cycled TEM samples. Further TEM study is required in order to unequivocally determine the effect of redox cycling on SOFC samples.

5. Conclusions and future work

The single-cell testing facilities at VPS were used to provide a baseline of the electrochemical performance degradation seen after redox cycling. Two types of electrochemical tests were performed: *I–V* curves and steady-state holds. After each redox cycle, during which air was directly passed over the fuel cell anode in order to oxidize it, the cell performance was evaluated and compared to the pre-redox performance values. The basic shapes of the *I–V* curves were unchanged after redox cycling. The OCV was slightly decreased after longer redox cycles (4 and 6 h), which indicates that some electrolyte fracture likely occurs. The cell voltage at 0.74 A/cm^2 and 750 °C was degraded by 0.089 ± 0.001 V or $10.9 \pm 0.1\%$ after a total redox time of 840 min. Slightly less cumulative degradation (0.072 ± 0.004 V or $8.9 \pm 0.6\%$) after redox cycling was seen for steady-state hold tests at 0.5 A/cm2, 54% fuel utilization and 750 °C.

Scanning and transmission electron microscopy were used to characterize the effect of redox cycling on fuel cell microstructure. SEM analysis showed that both the AFL and anode substrate layers were initially quite dense in the as prepared sample, but were made significantly more porous by reduction. After reoxidation, the samples were again quite dense and the NiO particles in the anode substrate appeared spongy with much smaller pores than in as prepared samples. Upon rereduction the microstructure was very similar to that seen in reduced samples.

TEM was used to characterize the microstructural changes seen in the anode substrate during redox cycling. During reduction, Ni crystals grew epitaxially on NiO and the overall Ni grain size remained the same as the consumed NiO. During reduction, the amount of intergranular porosity increased and very fine (50 nm) intragranular pores were formed throughout the Ni grains. Upon reoxidation, fine (<100 nm), randomly oriented grains of NiO were formed. The grain refinement that occurred upon reoxidation was likely due to the large number of intragranular pores that were produced upon reduction, which served as nucleation sites. Rereduced samples were also very fine grained (<200 nm) and contained significant amounts of small intergranular porosity. The YSZ grains were unaffected by the redox cycles.

The baseline of cell redox tolerance and redox induced microstructural changes, developed in this study, will be combined with information from previous kinetic studies [4] to develop cells with a modified anode microstructure and enhanced redox tolerance. Further TEM studies will be performed to more thoroughly examine the effect of redox cycling on overall SOFC microstructure and to look at the effect of redox cycling on the AFL in more depth.

Acknowledgements

The authors would like to thank Versa Power Systems Ltd. (VPS) for providing samples, access to testing facilities and funding. The Alberta Energy Research Institute (COURSE) and the Natural Sciences and Engineering Research Council (NSERC) of Canada are also acknowledged for providing financial assistance. Finally we would like to thank Dale Steedman, Murray Tilleman, Tahir Joia and Anqiang He for their assistance.

References

[1] N. Tikekar, T. Armstrong, A. Virkar, in: S.C. Singhal, M. Dokiya (Eds.), Proceedings of the Solid Oxide Fuel Cells VIII, The Electrochemical Society Proceedings Series, 2003, p. 670.
[2] D. Fouquet, A.C. Muller, A. Weber, E. Ivers-Tiffee, Ionics 8 (2003) 103.
[3] G. Stathis, D. Simwonis, F. Tietz, A. Moropoulou, A. Naoumides, J. Mater. Res. 17 (2002) 951.

[4] D. Waldbillig, A. Wood, D.G. Ivey, Solid State Ionics 176 (2005) 847.
[5] E. Tang, F. Martell, R. Brulé, K. Marcotte, B. Borglum, in: S.C. Singhal, M. Dokiya (Eds.), Proceedings of the Solid Oxide Fuel Cells VIII, The Electrochemical Society Proceedings Series, 2003, p. 935.
[6] K. Tu, J.W. Mayer, L.C. Feldman, Electronic Thin Film Science for Electrical Engineers and Materials Scientists, Macmillan, New York, 1976, pp. 167–174.
[7] H. Kuhlenbeck, H.J. Freund, in: D.A. King, D.P. Woodruff (Eds.), Growth and Properties of Ultrathin Epitaxial Layers, Elsevier, Amsterdam, 1997, Chapter 9.